Atmos. Chem. Phys. Discuss., 12, 15503–15540, 2012
www.atmos-chem-phys-discuss.net/12/15503/2012/
doi:10.5194/acpd-12-15503-2012

Atmospheric Chemistry and Physics Discussions

Detection in the summer polar stratosphere of air plume pollution from East Asia and North America by balloon-borne in situ CO measurements

G. Krysztofiak[1], R. Thiéblemont[1], N. Huret[1], V. Catoire[1], Y. Té[2], F. Jégou[1], P. F. Coheur[4], C. Clerbaux[3,4], S. Payan[2], M. A. Drouin[1], C. Robert[1], P. Jeseck[2], J.-L. Attié[5,6], and C. Camy-Peyret[2]

[1]LPC2E, UMR7328 CNRS-Université d'Orléans, 3A Avenue de la Recherche Scientifique, 45071 Orléans Cedex 2, France
[2]LPMAA, UMR7092 UPMC Univ. Paris 06, CNRS, IPSL, 75005, Paris, France
[3]UPMC Univ Paris 06 & Université Versailles St-Quentin, CNRS/INSU UMR8190, LATMOS-IPSL, Paris, France
[4]Spectroscopie de l'Atmosphère, Chimie Quantique et Photophysique, Université Libre de Bruxelles (ULB), Brussels, Belgium
[5]CNRM-GAME, Météo-France and CNRS, URA1357, Toulouse, France
[6]Laboratoire d'Aérologie, Université de Toulouse and CNRS, UMR5560, Toulouse, France

Received: 26 March 2012 – Accepted: 4 June 2012 – Published: 18 June 2012

Correspondence to: G. Krysztofiak (gisele.krysztofiak@cnrs-orleans.fr)

Published by Copernicus Publications on behalf of the European Geosciences Union.

ACPD

12, 15503–15540, 2012

Abstract

The SPIRALE and SWIR balloon-borne instruments have been launched in the Arctic polar region (near Kiruna, Sweden, 67.9° N, 21.1° E) during summer on 7 and 24 August 2009 and on 14 August 2009, respectively. The SPIRALE instrument performed in situ measurements of several trace gases including CO and O_3 between 9 and 34 km height, with very high vertical resolution (~5 m). The SWIR-balloon instrument measured total and partial column of several species including CO. The CO stratospheric profile from SPIRALE on 7 August 2009 shows some specific structures with strong abundance of CO in the low levels (potential temperatures between 320 and 380 K, i.e. 10–14 km height). These structures are not present in the CO vertical profile of SPIRALE on 24 August 2009, for which the volume mixing ratios are typical from polar latitudes (~30 ppb). CO total columns retrieved from the IASI-MetOp satellite sounder for the three dates of flights are used to understand this spatial and temporal CO variability. SPIRALE and SWIR CO partial columns between 9 and 34 km are compared, allowing us to confirm that the enhancement of CO is localised in the stratosphere. The measurements are investigated also in terms of CO:O_3 correlations and with the help of several modelling approaches (trajectory calculations, potential vorticity fields, results of chemistry transport model), in order to characterize the origin of the air masses sampled. The emission sources are qualified in terms of source type (fires, urban pollution) using NH_3 and CO measurements from IASI-MetOp and MODIS data on board the TERRA/AQUA satellite. The results give strong evidence that the unusual abundance of CO on 7 August is due to surface pollution plumes from East Asia and North America transported to the upper troposphere and then entering the lower stratosphere by isentropic advection. This study highlights that the composition of low polar stratosphere in summer can be affected by anthropogenic surface emissions through long range transport.

ACPD

12, 15503–15540, 2012

1 Introduction

The polar stratosphere during summertime remains largely unexplored. Only few measurement campaigns such as POLARCAT (Jacob et al., 2010; Brock et al., 2011), POLARIS (Pierce et al., 1999) and SAMMOA (Orsolini, 2001) have been conducted, but they focussed more on spring and early summertime.

Large scale transport and mixing between air masses from different latitudes and altitude origins affect the distribution of trace gases and aerosols at polar latitudes, and can impact the stratospheric ozone budget. Consequently, to understand these effects is crucial. Ozone change in the stratosphere affects the Earth radiative balance and this change modifies the stratospheric circulation (Baldwin et al., 2007, Forster et al., 2005). In the framework of the International Polar Year, the StraPolÉté project started on January 2009 (http://strapolete.cnrs-orleans.fr/). A successful balloon-borne campaign took place from Esrange near Kiruna (67.9° N, 21.1° E, Sweden) from 2 August to 12 September 2009 with eight balloon flights. One objective of the StraPolÉté project was to combine balloon measurements, satellite observations and modelling studies to characterize the dynamical state of the summer stratosphere in the polar region.

Polar atmosphere has been believed to be very clean for long time. The polar atmosphere becomes, however, more and more polluted due to the increase of the pollutant emissions at Northern mid-latitudes, followed by the long scale transport of the resulting pollution plumes (Raatz et al., 1984; Rinke et al., 2004). Carbon monoxide (CO) is one of these pollutants. Industrial processes, incomplete combustion, biomass burning and methane oxidation are the main sources of CO in the troposphere, while reaction with OH is the main sink. CO plays an important role in the tropospheric oxidation capacity and in the production of tropospheric ozone, depending on the NO_x quantities. CO has a chemical lifetime of around 2 months in the troposphere, allowing for possible direct transport into the stratosphere. CO is a good chemical tracer and, correlated with O_3, is a powerful tool to study the exchange between troposphere and stratosphere (Fischer et al., 2000; Hoor et al., 2002; Brioude et al., 2006). Depending on the

ACPD
12, 15503–15540, 2012

latitude, the typical tropospheric CO volume mixing ratios can vary from 40 to 200 ppb (Seinfeld and Pandis, 2006), with higher values in the Northern Hemisphere than in the Southern Hemisphere. The East Asia region is a large and increasing source of CO (Elliott et al., 1997; Akimoto et al., 2003). The intercontinental transport of CO pollution from that area can impact the troposphere and the stratosphere of different regions such as North America (Berntsen et al., 1999; Jaffe et al., 1999; Cooper et al., 2004) or Europe (Stohl et al., 2007; Fiedler et al., 2009). Indeed, East Asia is characterised by important transport from the boundary layer to the upper troposphere in air streams associated with mid-latitude cyclone called warm conveyor belt (WCB; Stohl et al., 2001; Liang et al., 2004). WCB is thought to be the primary mechanism for fast intercontinental transport of air plume pollution (Cooper et al., 2004). Stohl et al. (2007) and Liang et al. (2004) reported in particular the transport of polluted air masses across the Central North Pacific atmosphere to North America, and then Europe via WCB.

Very recently, Roiger et al. (2011) reported case studies of trace gas export from East Asia, across the North Pole to Greenland lowermost stratosphere (11.3 km altitude) via WCB. Most of the previous studies on the CO transport into the polar stratosphere used satellite measurements or airborne data (Harrigan et al., 2011; Roiger et al., 2011). In the present study, balloon-borne in situ measurements with high vertical resolution by SPIRALE (French acronym for infrared absorption spectroscopy by embarked tunable laser diodes) instrument (Moreau et al., 2005) reveal unusual CO abundance in the lower stratosphere at the beginning of August 2009. These measurements are compared to others performed during the campaign, on 24 August 2009 by SPIRALE and on 14 August 2009 by the SWIR-balloon (Short Wave Infra Red Fourier transform spectrometer in nadir-looking) instrument (Té et al., 2002), and to IASI (Infrared Atmospheric Sounding Interferometer) (Clerbaux et al., 2009), satellite data. The high abundance of CO measured is investigated in terms of latitude and altitude origins using modelling approach. The CO sources (natural and/or anthropogenic) are examined using NH_3 measurements from IASI and fire detection from MODIS (MODerate

ACPD
12, 15503–15540, 2012

resolution Imaging Spectroradiometer) instrument (Giglio et al., 2003) on Terra-Aqua satellite.

The instruments and models descriptions used to perform this study are summarised in Sect. 2. Section 3 presents the CO observations performed during the polar summer 2009 and their comparisons with satellite data. Using potential vorticity fields and trajectory calculations, we analyze the air masses origin sampled. Finally, in the discussion section we qualify the partitioning between tropospheric and stratospheric air using CO:O_3 correlation, we characterize the source of pollutants (natural/anthropogenic), and we conclude on the emission source locations (Asia/North America).

2 Instrument and model description

2.1 Balloon-borne instruments

Eight balloon-borne instruments have been launched during the campaign between 2 August and 12 September 2009 from ESRANGE (Swedish Space Corporation) close to Kiruna (67.9° N, 21.1° E, Sweden). Among these flights, the SPIRALE instrument flew twice, once on 7 August (hereafter flight SPF07), and on another occasion on 24 August, (flight SPF24). The SWIR-balloon instrument flew on 14 August (flight SWF14).

SPIRALE is a spectrometer with six tunable laser diodes for in situ measurements of trace gas species from the upper troposphere to the middle stratosphere (~34 km height). A detailed description of the instrument can be found in a previous paper (Moreau et al., 2005). In brief, the absorption of six laser beams in the mid-infrared region (3–8 µm), takes place between two mirrors distant of 3.50 m in a multipass optical Herriott cell located at the extremities of a deployable mast below the gondola, leading to a path length of 430.5 m. Several species, such as O_3, N_2O, CH_4, HCl, NO_2, HNO_3 and CO were measured with high frequency sampling (~1 Hz), which leads to a vertical resolution of a few meters (3 to 5 m), depending on the vertical velocity of

ACPD
12, 15503–15540, 2012

the balloon. The overall uncertainties take into account the random and systematic errors, combined as the square root of their quadratic sum. The two main sources of random errors are the fluctuations of the laser background emission signal and the signal-to-noise ratio. At low altitudes (<20 km), these are the main contributions to overall uncertainties. Systematic errors originate essentially from the laser line width (an intrinsic characteristic of the laser diode), which contributes more at lower pressure than at higher pressure (lower altitude). For CO, the overall uncertainty is on average 2.5 % (with a standard deviation of 1.8 %) below 15 km, increasing to 6 % at 17 km. For O_3, the overall uncertainty significantly decreases from 50 % at 13 km, to 10 % at 15 km, and 4 % at 17 km. Absorption micro-windows for both flights were 2123.55–2123.80 cm^{-1} for carbon monoxide and 2123.40–2123.54 cm^{-1} for ozone. The following time sequences characterized the two SPIRALE flights

- During SPF07, the first flight on 7 August 2009, the SPIRALE measurements started at 01:26 UT, i.e. 03:26 LT. The balloon reached the maximum altitude of 34.2 km (7.28 hPa) at 03:20 UT. The descent phase started at 03:32 UT and the measurements ended at 06:00 UT at 16.1 km (106.9 hPa).

- For SPF24, the second flight on the night of 24 to 25 August 2009, the measurements started at 20:50 UT and reached the maximum altitude of 34.1 km (6.9 hPa) at 22:30 UT. The descent phase started at 23:26 UT at 33.7 km and the measurements ended at 01:36 UT at 16.7 km (94 hPa).

For both flights, retrievals of the species volume mixing ratios (vmr) have been performed using ascent and descent phases. The study is focussed on the layer below 16 km altitude and thus only the ascent profiles allow studying this part of the atmosphere.

SWIR-balloon is an extended version in the short wave infrared domain of the IASI-balloon instrument (Té et al., 2002). This instrument is an infrared remote sensing instrument based on a Fourier Transform interferometer. The interferometer is associated with two InSb detector to cover both thermal infrared (3–5 µm) and SWIR (1.8–2.4 µm)

ACPD
12, 15503–15540, 2012

domains. The maximum optical path difference is fixed at 10 cm. In nadir-looking, SWIR-balloon observes the upwelling radiation which is composed of several contributions from the Earth surface emission, the emission and absorption of atmospheric constituents, the emission of the clouds and the reflected solar radiation. The recorded atmospheric spectra are radiometrically calibrated using two reference sources (Revercomb et al., 1988; Té et al., 2009). The LPMAA Atmospheric Retrieval Algorithm LARA (Clerbaux et al., 1999) is used to retrieve from the spectra total columns (from ground to 34 km, the gondola height) of CO, O_3, OCS, CO_2, N_2O and H_2O. For the CO retrieval, the spectral window from 2149 to 2171 cm^{-1} was used. In addition to CO, the contribution of the six atmospheric species H_2O, CO_2, O_3, N_2O, CH_4, and OCS has been taken into account. The main interfering species in this spectral window are H_2O, O_3 and N_2O. For the other three constituents, the absorption signals are comparable to the noise level. The SWIR-balloon instrument was flown during the campaign on 14 August 2009 at 09:26 UT for 5 h 58 min and covered the distance from the position (68.1° N, 21.0° E) for the first spectrum acquired at float to the last position (68.4° N, 20.6° E) before the balloon cut-off. The altitude at float varied between 34.0 km and 34.4 km from onboard GPS data.

2.2 Satellite instruments

Satellite data are used to interpret balloon measurements. IASI on board MetOp satellite allows for interpreting the evolution of CO spatial distribution and MODIS (MODerate resolution Imaging Spectroradiometer) on TERRA/AQUA allows for locating the fires.

The polar-orbiting MetOp-A, launched on 19 October 2006, is the first of three successive MetOp satellites. The IASI-MetOp instrument is a nadir-looking high resolution Fourier Transform Spectrometer (FTS). It is designed to provide atmospheric temperature and water vapour profiles for operational meteorology. Atmospheric concentrations of several key species important to climate forcing and atmospheric chemistry monitoring can be derived from IASI radiance measurements (Clerbaux et al., 2009), including

ACPD
12, 15503–15540, 2012

a variety of reactive compounds in fire or volcanic plumes (Clarisse et al., 2011). In addition, IASI-MetOp offers an excellent horizontal coverage due to its across track swath width of 2200 km, allowing for global coverage twice a day, with a field of view sampled by 2 × 2 circular pixels each with a 12 km footprint diameter at nadir. IASI-MetOp measures CO on a global scale. CO total columns and vertical profiles (18 tropospheric layers and an additional upper layer) are retrieved in near real time from the nadir radiance spectra using the FORLI fast radiative transfer and retrieval software (George et al., 2009, Hurtmans et al., 2012). Here we also use NH_3 total columns (Coheur et al., 2009) retrieved using a similar approach but restricted only to scenes where its spectral signature was unambiguously detected using a simple brightness temperature difference approach. Although this NH_3 product has not yet been validated, it is worth stressing that the total columns are overall consistent with those retrieved locally using a full line-by-line radiative transfer modelling (Clarisse et al., 2010).

MODIS (Giglio et al., 2003) on NASA Terra (MOD14) and Aqua (MYD14) satellites detects a wide spectral range of electromagnetic energy spread in 36 spectral bands ranging from 0.405 to 14.385 µm. We use the fire and thermal anomalies from climate modelling grid fire products at 0.5° resolution. Fire detection is performed using a contextual algorithm (Giglio et al., 2003) that exploits the strong emission of mid-infrared radiation from fires.

2.3 Model

Three models, namely FLEXTRA (Stohl et al., 1995), MIMOSA (Modèle Isentrope de transport Méso-échelle de l'Ozone Stratosphérique par Advection; Hauchecorne et al., 2002), and REPROBUS (REactive PRocesses ruling the Ozone BUdget in the Stratosphere; Lefèvre et al., 1994) have been used to calculate air mass trajectories, potential vorticity maps and chemistry scheme, respectively.

FLEXTRA is a Lagrangian atmospheric trajectory model, developed at the Institute of Meteorology and Geophysics University of Vienna to compute trajectories from meteorological fields of the European Centre of Medium-Range Weather Forecasts

ACPD
12, 15503–15540, 2012

(ECMWF). We used the ERA-Interim reanalysis fields (Dee et al., 2011) with an horizontal resolution of 1° × 1°, 60 vertical levels, and every 3 h. Clusters of three-dimensional backward trajectories in a volume of size 0.5° × 0.5° along latitude and longitude and 500 m height have been performed.

Potential vorticity (PV) maps are calculated using the MIMOSA contour advection model. This model performs high resolution advection calculations based on the ERA-Interim reanalysis (Dee et al., 2011) of wind, pressure and temperature. MIMOSA initially computes the PV field at a resolution of 1.125° in latitude and longitude vertically interpolated on an isentropic surface. This field is then interpolated on an x-y grid centred on the North Pole with a horizontal resolution of 37 × 37 km (three grid points/degree) and advected with a time step of one hour. To preserve the homogeneity of the field, a regridding of the PV field on the original grid is calculated every 6 h. The information on diabatic changes in the PV field at large scales can be extracted from the ERA-Interim fields. For the MIMOSA model this is done by applying to the advected field a relaxation towards the ERA-Interim PV field calculations with a time constant of 10 days. This technique allows running continuously MIMOSA over periods of several months in order to follow the evolution of dynamical barriers and fine scale structures such as vortex remnants and tropical intrusions (Marchand et al., 2003; Durry and Hauchecorne, 2005; Huret et al., 2006; Thiéblemont et al., 2011).

The REPROBUS 3-D chemistry-transport model (Lefèvre et al., 1994; Jourdain et al., 2008) contains a detailed description of O_x, NO_x, HO_x, ClO_x, BrO_x and CHO_x chemistry. It calculates the chemical evolution of 55 species using 160 gas-phase reactions and 6 heterogeneous reactions. Reaction rates coefficients are taken from the recommendations of Sander et al. (2006). The photolysis rates are calculated at every time step using a look-up table from the Tropospheric and Ultraviolet Visible (TUV) model (Madronich et al., 1999). The REPROBUS model extends from the ground up to 0.1 hPa, with a vertical resolution varying from less than 1 km near the tropopause level to 2.2 km in the upper part of the stratosphere. The horizontal resolution used for this study is 2° latitude × 2° longitude. Zonally symmetric initial tracer fields are taken

ACPD
12, 15503–15540, 2012

from the two-dimensional model described by Bekki et al. (1993). To represent the CO variability over the Northern Hemisphere, a typical 2000 s MOPITT CO climatological analysis (Claeyman et al., 2010) with 2° × 2° lat-lon resolution was used to fix the monthly CO source at 500 hPa level. MOPITT CO data are referenced in numerous publications (see Deeter et al., 2003, 2010). Winds and temperatures (ERA-INTERIM) from ECMWF were used during the REPROBUS simulation to drive the transport of the stratospheric species and to compute their loss and production rates, respectively.

3 Measurements

One of the objectives of the StraPolÉté project was to study the origin of the polar stratospheric air in summer. This project combined both balloon-borne and satellite measurements with relevant dynamical models and chemistry-transport models.

3.1 CO column variability in August 2009

The CO total columns from IASI-MetOp are shown in Fig. 1, represented in coloured squares for all overpasses around the Kiruna region for the three flights (SPF07, SWF14 and SPF24). The locations of the SPIRALE instrument trajectories are shown in black (top and bottom panels), and the SWIR data are shown in coloured circles (middle plot). When comparing the three figures, it appears that IASI CO total columns are different for each date:

- On 7 August a mean CO total column of $(1.88 \pm 0.12) \times 10^{18}$ molecule cm^{-2} is observed by IASI-MetOp close to the SPF07 flight track and in the entire range of latitude-longitude presented.
- On 14 August, the IASI-MetOp CO total columns are comparable to the CO total column measurements of SWF14 (coloured circle). Indeed the mean CO total column from IASI is $(1.55 \pm 0.10) \times 10^{18}$ molecule cm^{-2}, where as the average column retrieved from the SWIR-balloon is $(1.64 \pm 0.08) \times 10^{18}$ molecule cm^{-2} at the

ACPD
12, 15503–15540, 2012

location of 68.2° N, 20.7° E. Note that the spatial and temporal co-location is less than 0.5° in latitude and in longitude for the closest overpass as compared to the SWF14 trajectory.

– On the night of 24 August, during SPF24, the IASI CO total columns reveal some high values in the East region, similar to those obtained on 7 August (Fig. 1a). However, in the vicinity of the SPF24 flight track, CO total columns are below 1.7×10^{18} molecule cm^{-2}.

The CO total column measured on 7 August is on average 20 % higher than the CO total columns on 14 August and on 24 August (close to the SPF24 flight track).

In order to derive information on the altitude range (stratosphere/troposphere) corresponding to the high CO total column values measured by IASI, we have calculated the CO partial columns from 9 to 34 km height (Table 1) measured by SPIRALE and SWIR-balloon instruments for the three balloon flights. It appears that whereas SWF14 and SPF24 partial columns are of the same order of magnitude, SPF07 partial column is around two times larger. Consequently, we deduce that the high SPF07 CO values are mainly located in the stratosphere between 9 km and 34 km.

3.2 Vertical distribution of CO from in situ measurements

The CO vertical profiles for both SPIRALE flights are displayed in Fig. 2. The cold points, which indicate the tropopause height (Holton et al., 1995), were located at 11.78 and 11.34 km height on 7 and 24 August, respectively. The SPF24 vertical profile presents a 30 ppb averaged volume mixing ratio (vmr) without any variation as a function of altitude. On the contrary, during SPF07, the CO profile presents strong variations and the vmr is higher by up to 60 ppb than the SPF24 vmr. This later profile is mainly characterized by two layers, one below 12.6 km (below 350 K) with ~70–80 ppb CO (L1) located in the upper troposphere and lower stratosphere and the other between 12.6 and 14.3 km (350 K – 385 K) with ~40–50 ppb CO (L2) located in the stratosphere. In each layer, many thin structures are observed as evidences of atmospheric fine scale

ACPD
12, 15503–15540, 2012

disturbance. Above 14.5 km, both vertical profiles show similar features. The 30 ppb CO decreases smoothly with altitude for altitude higher than 14.5 km.

3.3 Data interpretation

3.3.1 Dynamical conditions

The stratospheric dynamical conditions are examined using the MIMOSA model results on 7, 14 and 24 August 2009 (Fig. 3).

- On 7 August during SPF07 (Fig. 3, top panels), a large low latitude air masses tongue (PV < 6 PVU) is located above Northern Europe at 340 K isentropic level (i.e. 12 km). At 380 K (i.e. 14 km), a thinner low latitude intrusion is recorded. The SPF07 vertical profile (Fig. 2, green), recording two high CO laminae located in the middle of L1 (13.5 km) and L2 (11.5 km), is in agreement with the MIMOSA maps where low PV intrusions are detected.
- On 14 August, high PV values (PV > 10 PVU) are observed above Kiruna (denoted by the white cross sign) at 340 and 380 K (Fig. 3, mid panel). This suggests the presence of typical polar air during the SWF14, which is confirmed by examining the SWIR results (Fig. 1b) having CO total column values typical from polar latitude.
- On 24 August finally, MIMOSA results at 340 K show that the launch of SPF24 occurred into a thin filament of high PV value located between two tongues of a low PV (lower latitude) air parcel. Such fine scale dynamical features are less pronounced at 380 K. The SPF24 vertical profile (Fig. 2, orange) and IASI CO total column (Fig. 1c, in the South-West part) displays that low CO values have been recorded, which is in agreement with the PV maps where polar air is detected above the flight position.

ACPD
12, 15503–15540, 2012

In summary, balloon measurements and MIMOSA maps are consistent with each other at the same isentropic levels. In particular, the MIMOSA model allows reproducing very thin dynamical structures such as polar filaments and low latitudes intrusions. However, the MIMOSA PV diagnosis does not inform on the origin of the 7 August high CO laminae. This aspect is investigated using the FLEXTRA trajectory calculation model.

3.3.2 Trajectory calculations

To investigate the origin of the polluted air masses sampled during SPF07 compared to the background air sampled during SPF24, we have calculated ten days 3-D backward trajectories (Fig. 4) for three clusters corresponding to the top and bottom of layer L1 (squares A and B in Fig. 2) and to the middle of the layer L2 (square C in Fig. 2). The backward trajectories of the air masses are coupled with the ERA-Interim horizontal wind module denoted by the $30\,m\,s^{-1}$ and $50\,m\,s^{-1}$ black isocontours at 225, 200 and 150 hPa pressure levels roughly corresponding to the 11.25, 12.0 and 13.5 km altitudes.

Figure 4 reveals that the air masses trajectories have been very different before reaching flight locations. The SPF24 (Fig. 4, right column) shows that during their 10 days transport, air masses remained confined northward of the jet stream (strong wind cells) in the polar region. The a, b and c panels altitude heights (illustrated by the colour code) remained roughly constant along the trajectories around 11.25, 12.0 and 13.5 km respectively (Fig. 4, right column). These trajectories analyses suggest that the SPF24 vertical profile results from isentropic transport confined in low stratosphere polar region, which is in good agreement with the low CO values measured by the various instruments.

In comparison, the SPF07 air masses trajectories (Fig. 4, left column) depict a very different aspect. The a panel (11.25 km, L1 bottom) shows that high vertical transport occurred above North East America and East Asia allowing several trajectories to rise from the ground to 10 km in few days. Such typical feature suggests the presence of a high convective activity in both regions. Following this quick ascent, the trajectories

ACPD
12, 15503–15540, 2012

are seen to be eastward advected along the horizontal wind cells maximum characterizing the upper tropospheric jet stream. On the b panel (12.0 km, L1 top), the strong influence of the jet stream also allows the air masses advection from mid-latitudes to the balloon flight location. However, along this trajectories cluster, no strong upward transport is detected, in contrast with the a panel. The height evolution reveals that the trajectories remained in the 10–14 km altitude range. The c panel (13.5 km, L2) shows that the air masses are subjected to a different transport regime, by comparison with the a and b panels. The influence of the jet stream on horizontal transport appeared again although its signature starts to decrease at these heights. The c panel reveals that the 40 ppb of CO measured in the L2 layer are due to the sampling of an air intrusion coming from the mid-latitudes (North America) and being isentropically advected through the polar region along the 350–380 K potential temperature surfaces.

This transport analysis highlights that SPF07 has sampled very different air masses in the polar region, resulting in various long range transport regime. In the upper troposphere, fast transport from the mid-latitude ground (North East America and East Asia) to free troposphere occurred, followed by isentropic transport (for L1), whereas in the lowermost stratosphere isentropic transport of mid-latitude air masses from North America has occurred (L2). Both revealed a crucial influence of the jet stream in the advection processes. On the contrary, the typical polar air masses sampled by SPF24 (Fig. 4 right) do not undergo any influence of the upper tropospheric jet stream for all altitudes.

The air masses sources are discussed in the next section.

4 Discussion

4.1 O_3:CO correlation

Tracer-tracer correlations are a powerful diagnosis for stratospheric transport and mixing analysis (Hoor et al., 2002; Huret et al., 2006). In particular, we are interested in

ACPD
12, 15503–15540, 2012

the O_3:CO correlation in the upper troposphere – lower stratosphere (UTLS), which has also been used in recent studies for transport diagnoses (Fischer et al., 2000; Hoor et al., 2002; Pan et al., 2004; Pirre et al., 2008; Roiger et al., 2011). CO is mainly produced or emitted in the troposphere and smoothly decreases with altitude in the stratosphere, reaching a volume mixing ratio minimum of about 10–15 ppb around 19–22 km altitude. Unlike CO, O_3 is mainly produced in the stratosphere and has thus a low vmr in the troposphere (50–200 ppb). Consequently, without mixing between the stratosphere and the troposphere around the tropopause, the correlation between CO and O_3 is an "L"-shape. This is illustrated by the dashed lines in Fig. 5. The vertical line of the "L" is called stratospheric branch and its horizontal line the tropospheric branch. Figure 5 shows the correlation between CO and O_3 on 7 August (a) and 24 August (b) for SPF07 and SPF24. The correlations are divided in different parts, according to the layers L1 (340 K–350 K) and L2 (350 K–385 K) previously identified. The layer between 385 K and 500 K is accessible by balloons, which allows us to clearly identify the CO stratospheric value (~15 ppbv). For the SPF24, correlations points show a steep slope and are close to the stratospheric branch. This correlation indicates that no recent mixing with tropospheric air has occurred.

On the contrary, for the SPF07, the lower layer (L1) matches relatively closely the horizontal tropospheric branch. It means that mixing of stratospheric air with tropospheric air has occurred recently. The L2 correlation points present more variability, corresponding also to a mixing between stratospheric and tropospheric air. As explained in Sect. 3.3.2, the high concentration of CO detected by SPIRALE is due to an exchange of air between the mid-latitude air and the polar lower stratosphere by isentropic transport. It is well known (Hoskin et al., 1991) that this region, where isentropic surfaces intersect the tropopause, is favourable to the horizontal mixing of stratospheric and tropospheric air. According to Fischer et al. (2000), the isentropic mixing between tropospheric and stratospheric air is represented by "mixing lines" between the tropospheric and the stratospheric branches. In our case, this transport is represented by "mixing lines" between the polar correlation for SPF07 (point 2 in the zoom of

ACPD
12, 15503–15540, 2012

Fig. 5a) and the mid-latitude reference correlation (point 3 in the zoom of Fig. 5a) at the same isentropic surface level (potential temperature). Point 1 on the polar stratospheric branch was found by extrapolating the straight line corresponding to point 2 and 3. In our case, the mid-latitude reference correlation is represented by the North America O_3:CO correlation and the typical mid latitude CO and O_3 concentrations in summer are 60 ppb and 150 ppb, respectively according to the studies of Tilmes et al. (2010). From the different correlations at the two different latitudes (polar and North America latitudes) and the mixing lines, we can calculate the proportion of tropospheric mid-latitude air present in the polar stratosphere for SPF07. The CO concentration is constant along L2, on average 40–50 ppb. Consequently, we determined the proportion only for the 380 K isentropic surface. At this isentropic surface level, we calculated the ratio between the distance from the polar stratospheric branch (point 1) to the polar correlation at 380 K (point 2) and the distance between the polar stratospheric branch (point 1) and the mid-latitude reference correlation (point 3). On average, 67 % of mid-latitude air (located in the mid-latitude UTLS between 350 K and 380 K) is mixed with stratospheric polar air at 380 K for SPF07.

4.2 The L1 layer origin

The objective of this section is to characterize the CO sources (urban pollution and/or fires) responsible for the polluted L1 layer observed by SPIRALE on 7 August.

4.2.1 Anthropogenic and natural CO Sources

Figure 6 shows the evolution of IASI CO total column from 29 July (9 days before the flight) to 7 August in the Northern Hemisphere. At the end of July, the CO transport from East Asia is well illustrated in this figure and the localisation of the air masses (of L1) is highlighted by black circles (clusters A and B resulting from FLEXTRA simulation, Sect. 3.3.2). At the beginning, the CO plume is located between 120° E and 180° E over North East of Asia. It has CO total columns higher than 3.5×10^{18} molecule cm^{-2}

ACPD
12, 15503–15540, 2012

(Fig. 6a). Figure 6b illustrates the plume pollution transport across the Pacific Ocean from Asia (150° E, 40° N) to North America (150° W, 60° N) during two days (31 July and 1 August). Then the pollution crosses North America toward the Atlantic Ocean (Fig. 6c). CO total column values are lower than values found 6 days before but still significant ($>2.25\times10^{18}$ molecule cm^{-2}). Starting from 5 August 2009, a long tongue of CO with columns higher than 2.25×10^{18} molecule cm^{-2} appears over the Atlantic Ocean (in green colour in Fig. 6d). Two days before the intrusion of 7 August, the CO plume is located in the middle of the Atlantic Ocean (40–50° N) and over the Western Europe. Then the pollution intrusion crosses Northern Europe with CO total column between 2.00×10^{18} and 2.75×10^{18} molecule cm^{-2} on 7 August 2009.

Figure 6 reveals several areas of high CO concentration (with columns $>2.8\times10^{18}$ molecule cm^{-2}) along the air masses trajectory (black line), over North East of Asia and over North America. To identify the origin of the pollution, we used, in addition to CO, ammonia (NH_3) columns from IASI and fires detection from MODIS. Indeed, CO is mainly emitted from biomass burning, fuel consumption, industry and from in situ oxidation of organics (Seinfeld and Pandis, 2006). Agriculture and biomass burning are the main sources of NH_3 (Bouwman et al., 1997). Consequently, NH_3 and CO have only one source in common, biomass burning, whereas the other sources are quite incompatible. NH_3 total column coupled with other gas tracers such as CO has already been used by Coheur et al. (2009) to highlight the strong fires that have occurred in the Mediterranean Basin in August 2007. These authors showed the good correlation between the CO and NH_3 emissions when the Greek fires occurred. To know the geographical area of biomass burning from 10 to 5 days before the flight, NH_3 and CO maps are coupled with fire detection maps from MODIS shown in Fig. 7. The map comparison highlights two areas of biomass burning, one over North East Asia (130–160° E, 60–65° N) and the other one over North America (135–155° W, 60–65° N), located along the air masses trajectories as potentially sources of CO impacting directly the polar upper troposphere and lowermost stratosphere.

ACPD
12, 15503–15540, 2012

4.2.2 CO emission regional distribution determined by simulation

To evaluate the potential impact of these anthropogenic and natural sources, we have performed simulations using the REPROBUS CTM. The trajectory study has pointed out that two polluted regions contribute to the CO loading in the polar region: North East Asia and North America. To evaluate the relative weight of these two regional emissions, two different masks were applied on MOPITT CO analyses used by REPROBUS as CO source at 500 hPa. In simulations 1 and 2, only North-Eastern Asian (105–150° E, 20–45° N) and Northern America (75–120° W, 30–45° N) emissions were taken into account, respectively. Simulation 3 is a control run using the global MOPITT CO climatology. Figure 8 shows the spatial extension of both masks. The test results are shown in Table 2.

The first simulation tests the impact of the East Asia CO emission on the polar stratosphere. This simulation shows comparable maximum CO at 11.4 km altitude on 14 and 24 August with a 12.5 ppb mean value. In comparison, the value on 7 August is larger by 12 ppb. In the control simulation 3 case, this difference is increased by a factor of 4 (larger by 50.6 ppb). According to the FLEXTRA backward trajectories (Sect. 3.2.2, Fig. 4), we considered that on 24 August 2009 the air masses are coming only from the polar latitudes. Consequently, the proportion of air from East Asia for SPF24 is estimated to be insignificant. So, the difference between the 7 and 24 August for REPROBUS simulation 1, at 11.4 km altitude, is only due to the intrusion and we can calculate the proportion of air from East Asia. On average, 24 % of CO in the airmass present on 7 August 2009 over Kiruna originates from anthropogenic East Asia pollution according to REPROBUS model.

Similarly, simulation 2 tests the impact of North America emissions on polar stratosphere. As in the previous test, the CO vmr over Kiruna on 14 and 24 August are similar (32 ± 4 ppb, see Table 2), whereas the CO vmr on 7 August is larger by 36 ppb than the 24 August one. As previously, we can calculate the proportion of CO originating from North America. 72 % of CO in the airmass the air present on 7 August 2009 over Kiruna

ACPD
12, 15503–15540, 2012

originates from North America (75–120° W, 30–45° N) according to REPROBUS model. As a conclusion, we have identified that about 96 % of non polar air masses originate from East Asia and North America.

Some warning has to be mentioned with regards to air masses origin taken into account by these two tests. The REPROBUS CO concentrations are nudged by the monthly CO climatology at 500 hPa level. The CO at this level could have several origins corresponding to regional or long-range transport. All CO pollution coming from nearby regions (e.g. biomass burning in North America (135–155° W, 60–65° N) or CO transport across the Pacific Ocean, Liang et al., 2004) and crossing the mask have been taken into account in our calculation. So, the relative parts of the long-range transport have to be taken as maxima.

5 Conclusions and perspectives

Eight balloon flights have been launched during the StraPolÉté campaign between 2 August and 12 September 2009 from ESRANGE base (Swedish Space Corporation) close to Kiruna, Sweden. Among these flights, the SPIRALE instrument flew twice, on 7 August and on 24 August. In addition, the SWIR-balloon instrument flew on 14 August.

The SPIRALE balloon-borne instrument observations in the lower stratosphere on 7 August showed two layers of air with very high carbon monoxide concentrations (mixing ratio near 80 ppb), directly coupled with poleward intrusions from mid-latitudes. The layers extend over the potential temperature range 328–380 K (10–14 km), with the CO maximum of 80 ppb at 330 K (11.4 km). These CO data are consistent with the MIMOSA model showing a region of low PV in the range 340–380 K. The CO mixing ratio in the range 50–80 ppb is typical from mid-latitude values for 10–15 km altitude range. Ten days backward trajectories between 10.5 km and 15 km from Kiruna have been calculated. The simulations showed that air masses of the upper layer, extending from 12.6 km to 14 km, originate from North America latitude at high altitude (10–14 km), according to the FLEXTRA model. Air masses of the lower layer, below 12.6 km, originate

ACPD
12, 15503–15540, 2012

from East Asia and North America at low altitude (<4 km). CO total column satellite data from IASI-MetOp instrument for the three dates of flights are used to understand this spatial and temporal CO variability. In agreement with the balloon observations, IASI measures comparably low CO concentrations on 14 and 24 August and much higher values on 7 August. SPIRALE and SWIR CO partial columns between 9 and 34 km are compared and allow us to confirm that the enhancement of CO is localised in the stratosphere

The upper layer is associated with an intrusion of air into polar stratosphere from North America (30–40° N, 75–105° N) via isentropic transport along the 350–385 K level. The O_3:CO correlation of the two flights of SPIRALE confirmed that a recent mixing with tropospheric air occurred in this region on 7 August 2009.

We have also investigated the origin, evolution and transport of air masses of the lower layer (L1, i.e. below 12.6 km). The transport revealed the important role of the long scale trans-Pacific transport and in particular, the role of the jet stream. The plume pollution was ascending over West Pacific near Japan probably associated to the WCB. After the initial ascent, the plume crossed the North Pacific Ocean, North America, and the North Atlantic Ocean in a fast zonal flow, called jet stream. IASI-MetOp measurements were also used to detect where high CO concentration occurred and allowed us to provide information on the origins of CO source. The CO total column maps were coupled with NH_3 from IASI and fire detection from MODIS were used to detect anthropogenic area emission over East China and biomass burning regions over North East of Asia and North America as potential CO sources impacting the polar region.

In this study, only one case was described. However, during the August 2009, there were three other similar phenomena simulated by MIMOSA model, on 21, 26 and 28 August. Therefore, the 7 August 2009 intrusion might not be an isolate case. The climatology of the intrusions during several summers should be established as well as the impact of urban mid-latitude pollution on the Arctic regions. Studies have started using trajectories model to evaluate the impact of three regions, namely Europe, USA and East China on Arctic (e.g., Harrigan et al., 2011).

ACPD
12, 15503–15540, 2012

Acknowledgements. The authors thank the LPC2E technical team (L. Pomathiod, B. Gaubicher, G. Chalumeau, B. Coûté, T. Vincent and F. Savoie) for the SPIRALE instrument preparation, the LPMAA technical team (I. Pépin, C. Rouillé and P. Marie-Jeanne) for the SWIR-balloon instrument preparation, the CNES balloon launching team and the Swedish Space Corporation at Esrange for successful operations, and A. Hauchecorne and F. Lefèvre for making available the MIMOSA and REPROBUS models. The ETHER database (Pôle thématique du CNES-INSU-CNRS) and the "CNES sous-direction Ballon" are partners of the project. The StraPolÉté project was funded by the French "Agence Nationale de la Recherche" (ANR-BLAN08-1_31627), the "Centre National d'Etudes Spatiales" (CNES), and the "Institut Polaire Paul-Emile Victor" (IPEV). In general, we acknowledge the mission scientists and Principal Investigators who provided the data used in this research effort (MODIS). IASI has been developed and built under the responsibility of the CNES. It is flown on board the MetOp satellites as part of the EUMETSAT Polar System. The IASI L1 data are received through the EUMETCast near-real-time data distribution service. P. F. Coheur is Research Associate with F.R.S.-FNRS and its research is also funded by the Belgian State Federal Office for Scientific, Technical and Cultural Affairs and the European Space Agency (ESA-Prodex arrangement), and the Actions de Recherche Concertées (Communauté Française de Belgique). Cathy Clerbaux is grateful to CNES for scientific collaboration and financial support. L. Clarisse, J. Hadji-Lazaro, D. Hurtmans, M. George, Y. Ngadi and M. Van Damme are acknowledged for scientific development and maintenance of the CO and NH_3 products from IASI.

The publication of this article is financed by CNRS-INSU.

ACPD
12, 15503–15540, 2012

References

Akimoto, H.: Global Air Quality and Pollution. Science, 302, 1716–1719, 2003.

Baldwin, M. P., Dameris, M., and Shepherd, T. G.: How will the stratosphere affect climate change?, Science, 316, 1576–1577, 2007.

Bekki, S. and Pyle, J. A.: Potential impact of combined NO_x and SO_x emissions from future high speed civil transport aircraft on stratospheric aerosols and ozone, Geophys. Res. Lett., 20, 723–726, 1993.

Bekki, S. and Pyle, J. A.: A two-dimensional modeling study of the volcanic eruption of mount Pinatubo, J. Geophys. Res., 99, 861–869, 1994.

Berntsen, T. K., Karlsdottir, S., and Jaffe, D. A.: Influence of Asian emissions on hte composition of air reaching the North Western United States, J. Geophys. Res., 26, 2171–2174, 1999.

Bouwman, A. F., Lee, D. S., Asman, W. A. H., Dentener, F. J., Van Der Hoek, K. W., and Olivier, J. G. J.: A global high-resolution emission inventory for ammonia, Global. Biogeochem. Cy., 11, 561–587, 1997.

Brioude, J., Cammas, J.-P., and Cooper, O. R.: Stratosphere-troposphere exchange in a summertime extratropical low: analysis, Atmos. Chem. Phys., 6, 2337–2353, doi:10.5194/acp-6-2337-2006, 2006.

Brock, C. A., Cozic, J., Bahreini, R., Froyd, K. D., Middlebrook, A. M., McComiskey, A., Brioude, J., Cooper, O. R., Stohl, A., Aikin, K. C., de Gouw, J. A., Fahey, D. W., Ferrare, R. A., Gao, R.-S., Gore, W., Holloway, J. S., Hübler, G., Jefferson, A., Lack, D. A., Lance, S., Moore, R. H., Murphy, D. M., Nenes, A., Novelli, P. C., Nowak, J. B., Ogren, J. A., Peischl, J., Pierce, R. B., Pilewskie, P., Quinn, P. K., Ryerson, T. B., Schmidt, K. S., Schwarz, J. P., Sodemann, H., Spackman, J. R., Stark, H., Thomson, D. S., Thornberry, T., Veres, P., Watts, L. A., Warneke, C., and Wollny, A. G.: Characteristics, sources, and transport of aerosols measured in spring 2008 during the aerosol, radiation, and cloud processes affecting Arctic Climate (ARCPAC) Project, Atmos. Chem. Phys., 11, 2423–2453, doi:10.5194/acp-11-2423-2011, 2011.

Claeyman, M., Attié, J.-L., El Amraoui, L., Cariolle, D., Peuch, V.-H., Teyssèdre, H., Josse, B., Ricaud, P., Massart, S., Piacentini, A., Cammas, J.-P., Livesey, N. J., Pumphrey, H. C., and Edwards, D. P.: A linear CO chemistry parameterization in a chemistry-transport model: evaluation and application to data assimilation, Atmos. Chem. Phys., 10, 6097–6115, doi:10.5194/acp-10-6097-2010, 2010.

ACPD
12, 15503–15540, 2012

Clarisse, L., Shephard, M. W., Dentener, F., Hurtmans, D., Cady-Pereira, K., Karagulian, F., Van Damme, M., Clerbaux, C., and Coheur, P. F.: Satellite monitoring of ammonia: A case study of the San Joaquin Valley, J. Geophys. Res.-Atmos., 115, D13302, doi:10.1029/2009JD013291, 2010.

Clarisse, L., R'Honi, Y., Coheur, P. F., Hurtmans, D., and Clerbaux, C: Thermal infrared nadir observations of 24 atmospheric gases, Geophys. Res. Lett., 38, L10802, doi:10.1029/2011GL047271, 2011.

Clerbaux, C., Hadji-Lazaro, J., Payan, S., Camy-Peyret C., and Mégie, G.: Retrieval of CO columns from IMG/ADEOS spectra, IEEE T. Geosci. Remote., 37, 1657–1661, 1999.

Clerbaux, C., Boynard, A., Clarisse, L., George, M., Hadji-Lazaro, J., Herbin, H., Hurtmans, D., Pommier, M., Razavi, A., Turquety, S., Wespes, C., and Coheur, P.-F.: Monitoring of atmospheric composition using the thermal infrared IASI/MetOp sounder, Atmos. Chem. Phys., 9, 6041–6054, doi:10.5194/acp-9-6041-2009, 2009.

Coheur, P.-F., Clarisse, L., Turquety, S., Hurtmans, D., and Clerbaux, C.: IASI measurements of reactive trace species in biomass burning plumes, Atmos. Chem. Phys., 9, 5655–5667, doi:10.5194/acp-9-5655-2009, 2009.

Cooper, O. R., Forster, C., Parrish, D., Trainer, M., Dunlea, E., Ryerson, T., Hübler, G., Fehsenfeld, F., Nicks, D., Holloway, J., de Gouw, J., Warneke, C., Roberts, J. M., Flocke, F., and Moody, J.: A case study of transpacific warm conveyor belt transport: influence of merging airstreams on trace gas import to North America, J. Geophys. Res., 109, D23S08, doi:10.1029/2003JD003624, 2004.

Dee, D. P., Uppala, S. M., Simmons, A. J., Berrisford, P., Poli, P., Kobayashi, S., Andrae, U., Balmaseda, M. A., Balsamo, G., Bauer, P., Bechtold, P., M., Beljaars, A. C., van de Berg, L., Bidlot, J., Bormann, N., Delsol, C., Dragani, R., Fuentes, M., Geer, A. J., Haimberger, L., Healy, S. B., Hersbach, H., Holm, E. V., Isaksen, L., Kallberg, P., Kohler, M., Matricardi, M., McNally, A. P., Monge-Sanz, B. M., Morcrette, J.-J., Park, B.-K., Peubey, C., de Rosnay, P., Tavolato, C., Thepaut, J.-N., and Vitart, F.: The ERA-Interim reanalysis: configuration and performance of the data assimilation system, Q. J. Roy. Meteor. Soc., 137, 553–597, 2011.

Deeter, M. N., Emmons, L. K., Francis, G. L., Edwards, D. P., Gille, J. C., Warner, J. X., Khattatov, B., Ziskin, D., Lamarque, J. F., Ho, S. P., Yudin, V., Attié, J. L., Packman, D., Chen, J., Mao, D., Drummond, J. R.: Operational carbon monoxide retrieval algorithm and selected results for the MOPITT instrument, J. Geophys. Res., 108, 4399, doi:10.1029/2002JD003186, 2003

ACPD
12, 15503–15540, 2012

Deeter, M. N., Edwards, D. P., Gille, J. C., Emmons, L. K., Francis, G., Ho, S.-P., Mao, D., Masters, D., Worden, H., Drummond, J. R., and Novelli, P. C.: The MOPITT version 4 CO product: Algorithm enhancements, validation, and long-term stability, J. Geophys. Res., 115, D07306, doi:10.1029/2009JD013005, 2010.

Durry, G. and Hauchecorne, A.: Evidence for long-lived polar vortex air in the mid-latitude summer stratosphere from in situ laser diode CH4 and H2O measurements, Atmos. Chem. Phys., 5, 1467–1472, doi:10.5194/acp-5-1467-2005, 2005.

Elliott, S., Blake, D. R., Duce, R. A., Lai, C. A., McCreary, I., McNair, L. A., Rowland, F. S., Russell, A. G., Streit, G. E., and Turco, R. P.: Motorization of China implies changes in Pacific air chemistry and primary production, Geophys. Res. Lett., 24, 2671–2674, doi:10.1029/97GL02800, 1997.

Fiedler, V., Nau, R., Ludmann, S., Arnold, F., Schlager, H., and Stohl, A.: East Asian SO_2 pollution plume over Europe – Part 1: Airborne trace gas measurements and source identification by particle dispersion model simulations, Atmos. Chem. Phys., 9, 4717–4728, doi:10.5194/acp-9-4717-2009, 2009.

Fischer, H., Wienhold, G., Hoor, P., Bujok, O., Schiller, C., Siegmund, P., Ambaum, M., Scheeren, H. A., and Lelieveld, J.: Tracer correlations in the northern high latitude lowermost stratosphere: influence of cross tropopause masse exchange, Geophys. Res. Lett., 27, 97–100, 2000.

Foster, P. M. de F. and Joshi, M.: the role of halocarbons in the climate change of the troposphere and stratosphere, Clim. Change, 71, 249–266, doi:10.1007/s10584-005-5955-7, 2005

George, M., Clerbaux, C., Hurtmans, D., Turquety, S., Coheur, P.-F., Pommier, M., Hadji-Lazaro, J., Edwards, D. P., Worden, H., Luo, M., Rinsland, C., and McMillan, W.: Carbon monoxide distributions from the IASI/METOP mission: evaluation with other space-borne remote sensors, Atmos. Chem. Phys., 9, 8317–8330, doi:10.5194/acp-9-8317-2009, 2009.

Giglio, L., Descloitres, J., Justice, C. O., and Kaufman, Y. J.: An enhanced contextual firedetection algorithm for MODI S., Remote. Sens. Environ., 87, 273–282, 2003 and http://modis-fire.umd.edu, last access: December 2011.

Harrigan, D. L., Fuelberg, H. E., Simpson, I. J., Blake, D. R., Carmichael, G. R., and Diskin, G. S.: Transport of anthropogenic emissions during ARCTAS-A: a climatology and regional case studies, Atmos. Chem. Phys. Discuss., 11, 5435–5491, doi:10.5194/acpd-11-5435-2011, 2011.

ACPD
12, 15503–15540, 2012

Hauchecorne, A., Godin, S., Marchand, M., Heese, B., and Souprayen, C.: Quantification of the transport of chemical constituents from the polar vortex to midlatitudes in the lower stratosphere using the high-resolution advection model MIMOSA and effective diffusivity, J. Geophys. Res., 107, 8289, doi:10.1029/2001JD000491, 2002.

Holton, J. R., Haynes, P. H., Mcintyre, M. E., Douglass, A. R., Rood, R. B., and Pfister, L.: Stratosphere-troposphere exchange, Rev. Geophys., 33, 403–439, 1995.

Hoor P., Fischer, H., Lange, L., Lelieveld J., and Brunner, D.: Seasonal variation of a mixing layer in the lowermost stratosphere as identified by the CO-O_3 correlation from in situ measurements, J. Geophys. Res., 107, 4044, doi:10.1029/2000JD000289, 2002.

Hoskins, B. J.: Towards a PV-θ view of the general circulation. Tellus, 43AB, 27–35, 1991.

Huret, N., Pirre, M., Hauchecorne, A., Robert, C., and Catoire, V.: On the vertical structure of the stratosphere at midlatitudes during the first stage of the polar vortex formation and in the polar region in the presence of a large mesospheric descent, J. Geophys. Res., 111, D06111, doi:10.1029/2005JD006102, 2006.

Hurtmans, D., Coheur, P. F., Wespes, C., Clarisse, L., Scharf, O., Clerbaux, C., Hadji-Lazaro, J., George, M., and Turquety, S.: FORLI radiative transfer and retrieval code for IAS I. in press, J. Quant. Spectrosc. Rad. Transfer, 113, 1391–1408, doi:10.1016/j.jqsrt.2012.02.036, 2012.

Jacob, D. J., Crawford, J. H., Maring, H., Clarke, A. D., Dibb, J. E., Emmons, L. K., Ferrare, R. A., Hostetler, C. A., Russell, P. B., Singh, H. B., Thompson, A. M., Shaw, G. E., McCauley, E., Pederson, J. R., and Fisher, J. A.: The Arctic Research of the Composition of the Troposphere from Aircraft and Satellites (ARCTAS) mission: design, execution, and first results, Atmos. Chem. Phys., 10, 5191–5212, doi:10.5194/acp-10-5191-2010, 2010.

Jaffe, D., Anderson, T., Covert, D., Kotchenruther, R., Trost, B., Danielson, J., Simpson, W., Berntsen, T., Karlsdottir, S., Blake, D., Harris, J., Carmichael, G., and Uno, I.: Transport of Asian Air Pollution to North America, Geophys. Res. Lett., 26, 711–714, 1999.

Jourdain, L., Bekki, S., Lott, F., and Lefèvre, F.: The coupled chemistry-climate model LMDz-REPROBUS: description and evaluation of a transient simulation of the period 1980–1999, Ann. Geophys., 26, 1391–1413, doi:10.5194/angeo-26-1391-2008, 2008.

Lefèvre, F., Brasseur, G. P., Folkins, I., Smith, A. K., and Simon, P.: Chemistry of the 1991–1992 stratospheric winter: three-dimensional model simulations, J. Geophys. Res., 99, 8183–8195, 1994.

Liang, Q., Jaegle, L., Jaffe, D. A., Weiss-Penzias, P., Heckman, A., and Snow, J. A.: Long-range transport of Asian pollution to the Northeast Pacific: seasonal variations and transport

ACPD
12, 15503–15540, 2012

pathways of carbon monoxide, J. Geophys. Res., 109, D23S07, doi:10.1029/2003JD004402, 2004.
Madronich, S. and Flocke, S.: The role of solar radiation in atmospheric chemistry, in: Handbook of Environmental Chemistry, edited by: P. Boule, Springer-Verlag, Heidelberg, 1–26, 1999.
Marchand, M., Godin, S., Hauchecorne, A., Lefèvre, F., Bekki, S., and Chipperfield, M.: Influence of polar ozone loss on northern midlatitude regions estimated by a high-resolution chemistry transport model during winter 1999/2000, J. Geophys. Res., 108, 8326, doi:10.1029/2001JD000906, 2003.
Moreau, G., Robert, C., Catoire, V., Chartier, M., Camy-Peret, C., Huret, N., Pirre, M., Pomathiod, L., and Chalumeau, G.: A multispecies in situ balloon-borne experiment with six tunable diode laser spectrometers, Appl. Opt., 44, 5972–5989, 2005.
Orsolini, Y. J.: Long-lived tracer patterns in the summer polar stratosphere, Geophys. Res. Lett., 28, 3855–3858, 2001.
Pan, L. L., Randel, W. J., Gary, B. L., Mahoney, M. J., and Hintsa, E. J.: Definitions and sharpness of the extratropical tropopause: A trace gas perspective, J. Geophys. Res., 109, D23103, doi:10.1029/2004JD004982, 2004.
Pierce, R. B., Al-Saadi, J. A., Fairlie, T. D., Olson, J. R., Eckman, R. S., Grose, W. L., Lingenfelser, G. S., and Russell III, J. M.: Large-scale stratospheric ozone photochemistry and transport during the POLARIS Campaign, J. Geophys. Res., 104, 26525–26545, doi:10.1029/1999JD900395, 1999.
Pirre, M., Pisso, I., Marecal, V., Catoire, V., Mebarki, Y., and Robert, C.: Intrusion of recent air in midlatitude stratosphere revealed by in situ tracer measurements and trajectory calculations, J. Geophys. Res., 113, D11302, doi:10.1029/2007JD009188, 2008.
Raatz, W. E. and Shaw, G. E.: Long-range tropospheric transport of pollution aerosols in the Alaskan Arctic, J. Clim. Appl. Meteorol., 23, 1052–1064, 1984.
Revercomb, H. E., Buijs, H., Howell, H. B., LaPorte, D. D., Smith, W. L., and Sromovsky, L. A.: Radiometric calibration of IR Fourier transform spectrometers: solution to a problem with the high-resolution interferometer sounder, Appl. Opt., 27, 3210–3218, 1988.
Rinke, A., Dethloff, K., and Fortmann, M.: Regional climate effects of Arctic haze, Geophys. Res. Lett., 31, L16202, doi:10.1029/2004GL020318, 2004.
Roiger, A., Schlager, H., Schäfler, A., Huntrieser, H., Scheibe, M., Aufmhoff, H., Cooper, O. R., Sodemann, H., Stohl, A., Burkhart, J., Lazzara, M., Schiller, C., Law, K. S., and Arnold,

ACPD
12, 15503–15540, 2012

F.: In-situ observation of Asian pollution transported into the Arctic lowermost stratosphere, Atmos. Chem. Phys., 11, 10975–10994, doi:10.5194/acp-11-10975-2011, 2011.
Sander, S. P., Ravishankara, A. R., Golden, D. M., Kolb, C. E., Kurylo, M. J., Molina, M. J., Moortgat, G. K., Finlayson-Pitts, B. J., Wine, P. H., and Huie, R. E.: Chemical Kinetics and Photochemical Data for Use in Atmospheric Studies Evaluation Number 15, JPL Publication, 06–2, 2006.
Seinfeld J. H. and Pandis S. N.: Atmospheric Chemistry and Physics: from Air Pollution to Climate Change, Chapt. 7, Second edition, John Wiley & Sons Ed, Inc., New York, 2006.
Stohl, A.: A 1-year Lagrangian "climatology" of airstreams in the Northern Hemisphere troposphere and lowermost stratosphere, J. Geophys. Res., 106, 7263–7279, 2001
Stohl, A., Wotawa, G., Seibert, P., and Kromp-Kolb, H.: Interpolation errors in wind fields as a function of spatial and temporal resolution and their impact on different types of kinematic trajectories, J. Appl. Meteor., 34, 2149–2165, 1995.
Stohl, A., Forster, C., Huntrieser, H., Mannstein, H., McMillan, W. W., Petzold, A., Schlager, H., and Weinzierl, B.: Aircraft measurements over Europe of an air pollution plume from Southeast Asia – aerosol and chemical characterization, Atmos. Chem. Phys., 7, 913–937, doi:10.5194/acp-7-913-2007, 2007.
Té, Y., Jeseck, P., Camy-Peyret, C., Payan, S., Perron, G., and Aubertin, G.: Balloonborne calibrated spectroradiometer for atmospheric nadir sounding, Appl. Opt., 41, 6431–6441, 2002.
Té, Y., Jeseck, P., Pépin, I., and Camy-Peyret, C.: A method to retrieve blackbody temperature errors in the two points radiometric calibration, Infrared. Phys. Techn., 52, 187–192, doi:10.1016/j.infrared.2009.07.003, 2009.
Thiéblemont, R., Huret, N., Orsolini, Y. J., Hauchecorne, A., and Drouin, M.-A.: Frozen-in anticyclones occurring in polar Northern Hemisphere during springtime: Characterization, occurrence and link with quasi-biennial oscillation, J. Geophys. Res., 116, D20110, doi:10.1029/2011JD016042, 2011.
Tilmes, S., Pan, L. L., Hoor, P., Atlas, E., Avery, M. A., Campos, T., Christensen, L. E., Diskin, G. S., Gao, R. S., Herman, R. L., Hintsa, E. J., Loewenstein, M., Lopez, J., Paige, M. E., Pittman, J. V., Podolske, J. R., Proffitt, M. R., Sachse, G. W., Schiller, C., Schlager, H., Smith, J., Pelten, N., Webster, C., Weinheimer, A., and Zondlo M. A.: An aircraft-based upper troposphere lower stratosphere O_3, CO, and H_2O climatology for the Northern Hemisphere, J. Geophys. Res., 115, D14303, doi:10.1029/2009JD012731, 2010.

ACPD
12, 15503–15540, 2012

Table 1. Comparisons of the CO partial columns between 9 and 34 km altitude between SPIRALE and SWIR balloon instruments during summer 2009.

Date		Instrument	Column (9–34 km) (molecule cm^{-2})	Errors (molecule cm^{-2})
7 Aug 2009	SPF07	SPIRALE	2.90×10^{17}	±0.06
14 Aug 2009	SWF14	SWIR-balloon	1.30×10^{17}	±0.07
24 Aug 2009	SPF24	SPIRALE	1.58×10^{17}	±0.06

ACPD
12, 15503–15540, 2012

Table 2. CO volume mixing ratio (ppb) for the three flights, at 11.4 km altitude, for the three simulations. Simulation 1 is with a mask over East Asia, simulation 2 with a mask over North America and simulation 3 without any mask. See text (Sect. 4.2) for details.

Simulation	Region	CO (ppb) 7 Aug	CO (ppb) 14 Aug	CO (ppb) 24 Aug	CO (7 Aug)–CO(24 Aug)
1	East Asia	24.5	12.6	12.5	12.0 (24 %)*
2	North America	72.3	27.8	36.0	36.3 (72 %)*
3	World	80.3	33.3	29.8	50.6 (100 %)*

*Proportion of air from the source region over Kiruna on 7 August 2009.

ACPD
12, 15503–15540, 2012

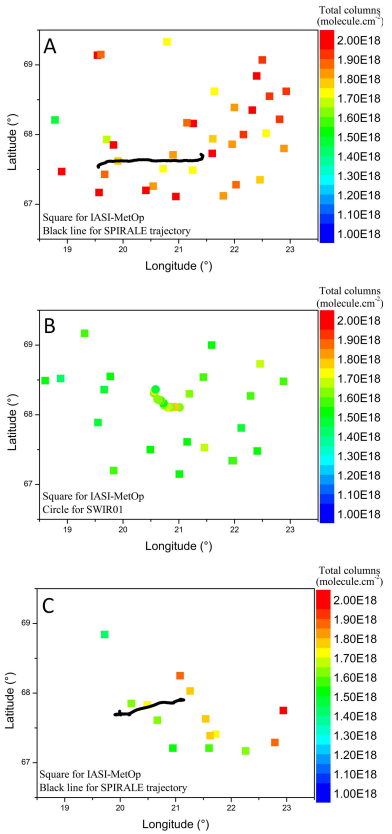

Fig. 1. Maps of CO total columns (molecule cm^{-2}) from IASI-MetOp satellite data, **(A)** on 7 August 2009, **(B)** on 14 August 2009 and **(C)** on 24 August 2009. IASI CO data are compared with balloon-borne data from SWIR01 instrument (coloured circles) on 14 August 2009, and the locations of the SPIRALE instrument trajectories are represented by the black solid line on **(A)** and **(C)**.

ACPD
12, 15503–15540, 2012

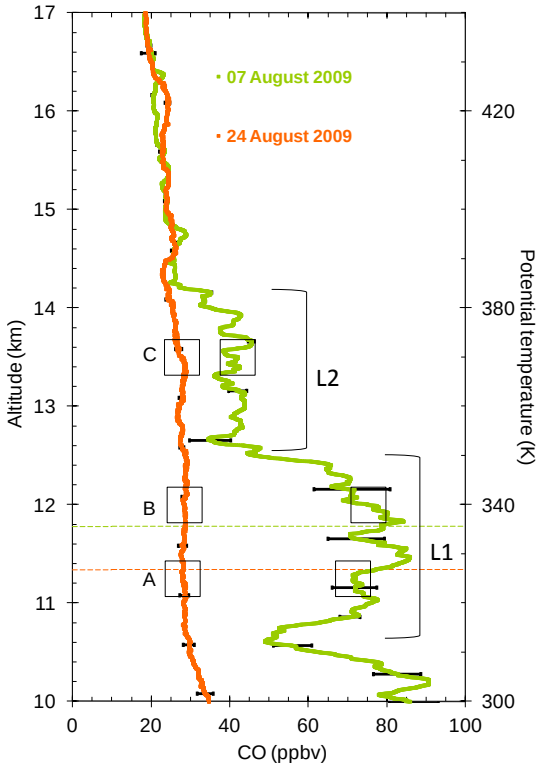

Fig. 2. SPIRALE measurements of CO volume mixing ratios (in ppb) with error bars above Esrange (67.9° N, 21.1° E, Sweden) on 7 August (green) and 24 August 2009 (orange). The horizontal dashed line represents the tropopause height for each flight. The squares named **(A)**, **(B)** and **(C)** represent the altitudes of the clusters for the backward trajectories. L1 and L2 indicate two different layers (see Sect. 3.2).

ACPD
12, 15503–15540, 2012

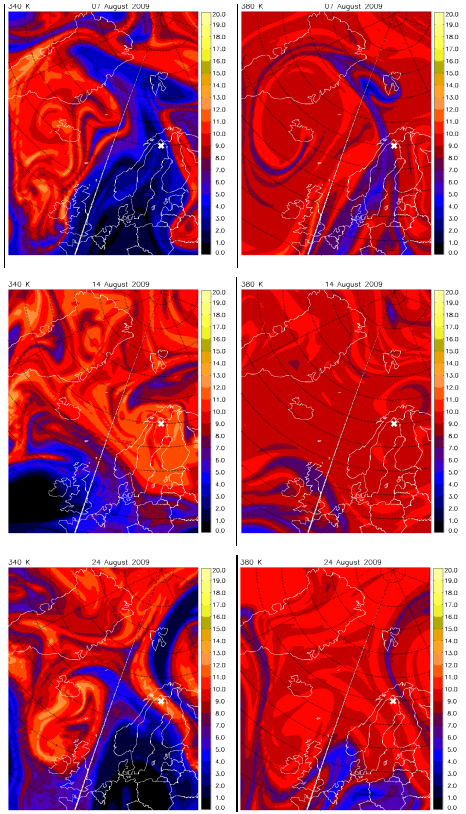

Fig. 3. Potential vorticity (1 PVU = 10^{-6} K m^2 kg^{-1} s^{-1}) from MIMOSA model at the 340 K level (left panels) and 380 K level (right panels) on 7 August 2009 at 00:00 UTC (top panels), on 14 August 2009 at 12:00 UTC (middle panels) and on 24 August 2009 at 18:00 UTC (bottom panels). The white cross sign shows the location of the balloon flights.

ACPD
12, 15503–15540, 2012

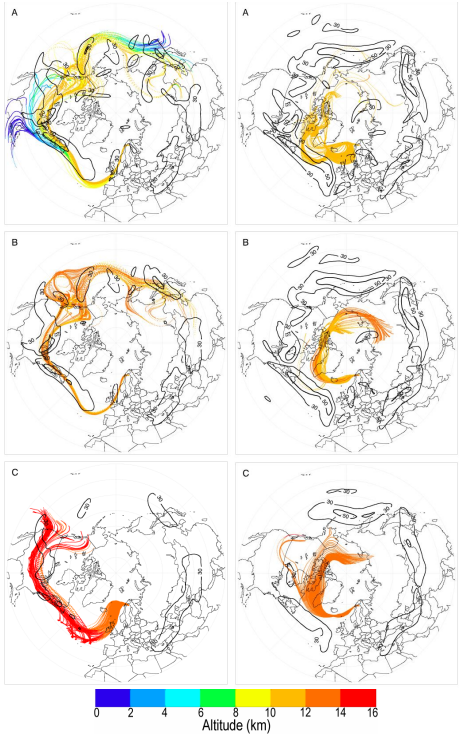

Fig. 4. Ten days backward trajectories calculated by the FLEXTRA model (Stohl et al., 1995) on 7 August 2009 (left panels) and on 24 August (right panels) for clusters centred in altitude at **(A)** 11.25 km, **(B)** 12.0 km, **(C)** 13.5 km, coupled with the ERA-Interim horizontal wind module on 7 August 2009 (black solid line) (m s^{-1}) at **(A)** 225 hPa, **(B)** 200 hPa and **(C)** 150 hPa.

ACPD
12, 15503–15540, 2012

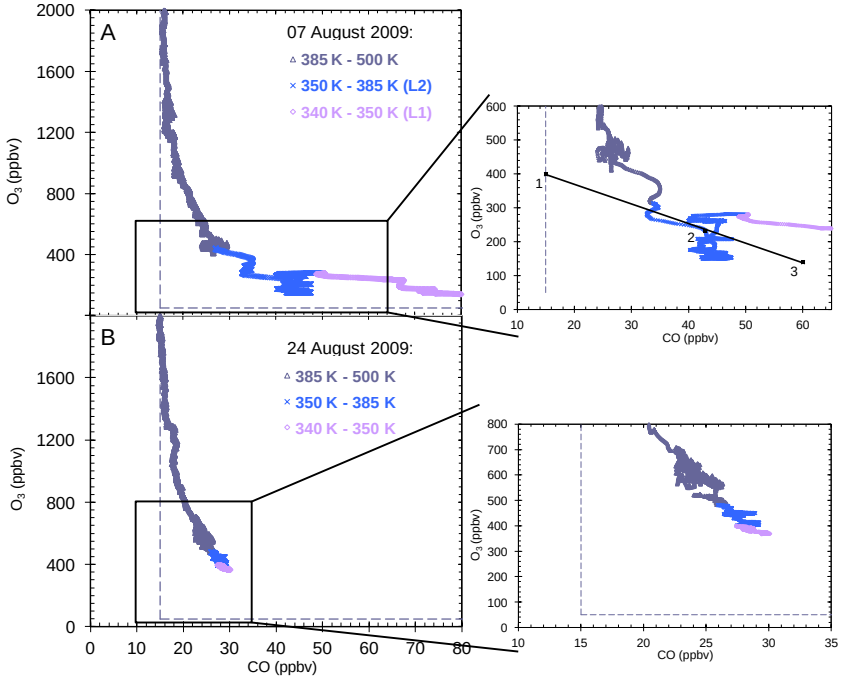

Fig. 5. Correlation between O_3 and CO from SPIRALE in situ measurements, **(A)** on 7 August 2009, and **(B)** on 24 August 2009. The colours correspond to different intervals of potential temperature. The vertical dashed line represents the stratospheric branch and the horizontal one represents the tropospheric branch. The black squares (**A** zoom) correspond to the 380 K level: (1) for stratospheric branch, (2) for SPIRALE measurement, and (3) for mid-latitude typical correlation (from Tilmes et al., 2010). The solid black line corresponds to the mixing line at 380 K.

ACPD
12, 15503–15540, 2012

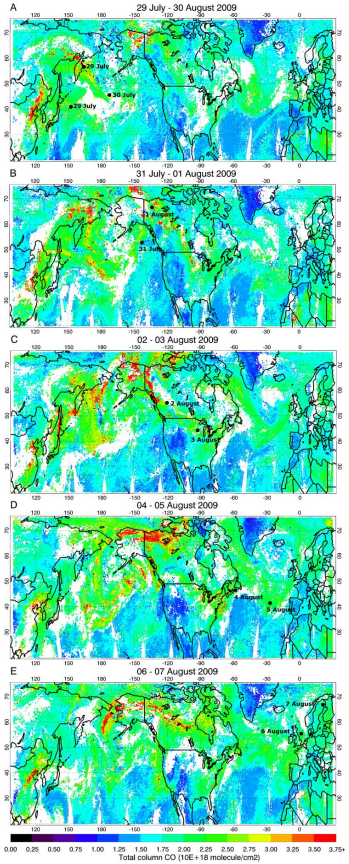

Fig. 6. CO total column (molecule cm^{-2}) from IASI-MetOp satellite evolution from 29 July 2009 **(A)** to 7 August 2009 **(E)**. The circles indicate the location of the air masses before the flight day (cluster **(A)** and **(B)** resulting from FLEXTRA simulation).

ACPD
12, 15503–15540, 2012

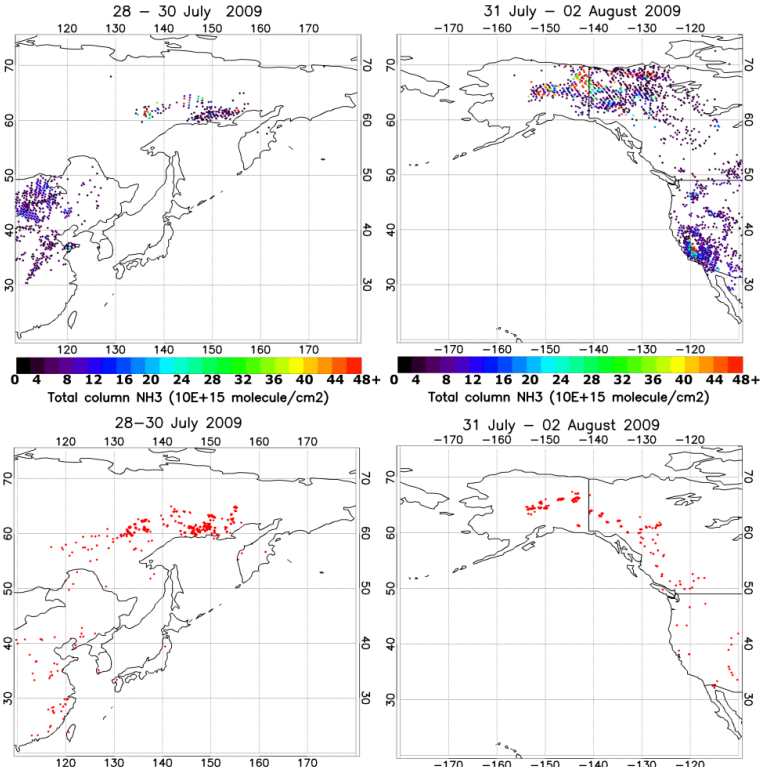

Fig. 7. NH_3 total column (molecule cm^{-2}) (top panels) from the IASI instrument and fire detection by MODIS (bottom panels) (each red point symbolizes a fire location) from 29 to 30 July 2009 over North-East of Asia (left panels) and from 31 July to 2 August 2009 over North America (right panels).

ACPD
12, 15503–15540, 2012

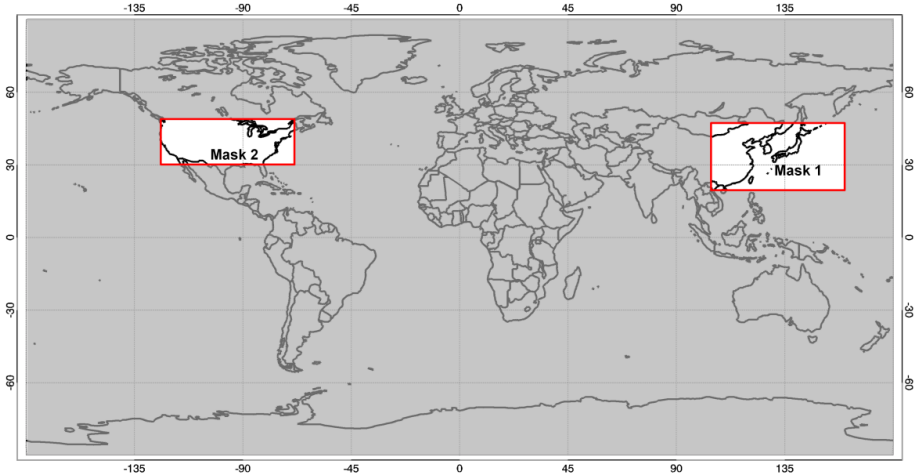

Fig. 8. Spatial extensions of mask 1 and mask 2: the CO emissions in the grey part are not taken into account for simulation 1 or 2, depending on the mask.

ACPD
12, 15503–15540, 2012